Analysis of the neutron A_N and the paper draft

Aug 29
Minho Kim

Analysis flow

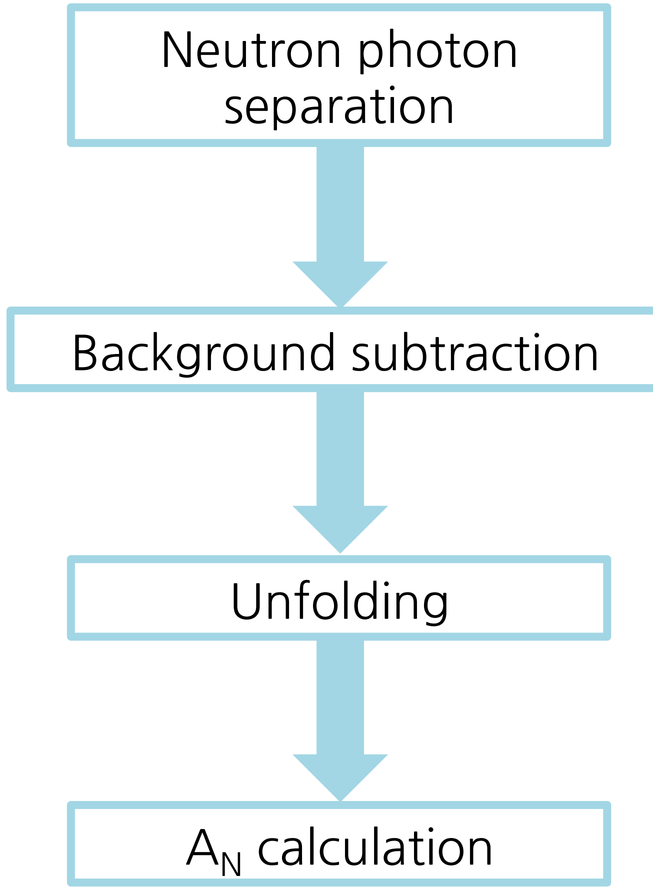

Outline of the neutron paper (for PRD)

Subject

Measurement of the transverse single-spin asymmetry for forward neutron production in a wide p_T range in polarized $p+p$ collisions at $\sqrt{s}=510$ GeV

M. H. Kim,[1] O. Adriani,[2,3] E. Berti,[2,3] L. Bonechi,[3] R. D'Alessandro,[2,3] Y. Goto,[1,4] B. Hong,[5] Y. Itow,[6,7] K. Kasahara,[8] Y. Kim,[9] S. H. Lee,[9] H. Menjo,[6] I. Nakagawa,[1,4] S. Oh,[9] T. Sako,[10] N. Sakurai,[11] K. Sato,[6] R. Seidl,[1,4] K. Tanida,[12] S. Torii,[13] and A. Tricomi[14,15,16]
(RHICf Collaboration)

J. H. Lee,[17] T. Ljubicic,[17] G. Mitsuka,[18] and A. Ogawa[17]

Contents

I. INTRODUCTION

II. THE RHICF EXPERIMENT

III. EVENT RECONSTRUCTION AND SELECTION

IV. BACKGROUND SUBTRACTION AND UNFOLDING

V. RESULTS

VI. SUMMARY

I. INTRODUCTION

I. INTRODUCTION

With the discovery of a large transverse single-spin asymmetry (A_N) for forward neutron production [1] from the first polarized $p+p$ collisions at a center of mass energy ($\sqrt{s}$) of 200 GeV at RHIC, the spin-dependent production mechanism of the forward neutron has attracted great interest over ten years. The A_N is defined by a left-right cross section asymmetry as

$$A_N = \frac{d\sigma_{\rm left} - d\sigma_{\rm right}}{d\sigma_{\rm left} + d\sigma_{\rm right}}, \quad (1)$$

where $d\sigma_{\rm left(right)}$ is the particle production cross section in the left (right) side of the beam polarization. A_N of the forward particle produced at pseudorapidity (η) larger than 6 is especially important to study the production mechanism of the particle in the region where the perturbative quantum chromodynamics is not applicable. The discovery inspired the PHENIX experiment to measure the neutron A_N at $\sqrt{s} = 62$ GeV, 200 GeV, and 500 GeV [2] to study the kinematic dependence of the neutron A_N. One-pion-exchange (OPE) model [3–5], that successfully described the unpolarized forward neutron production [6], introduced an interference between spin flip π and spin nonflip a_1 exchange between two protons. This theoretical framework reproduced the PHENIX data reasonably well showing that the neutron A_N increased with increasing transverse momentum (p_T) with little energy dependence [7]. Recently, the A_Ns at $\sqrt{s} = 200$ GeV in Ref. [2] was extracted as functions of longitudinal momentum fraction (x_F) and p_T [8] and they showed the same tendency with the model calculations. Thus far the neutron A_N has been studied only in a narrow kinematic range in $p_T < 0.4$ GeV/c, the production mechanism of the forward neutron with higher $p_T > 0.4$ GeV/c has not been understood. Here we has extended the kinematic range of the previous measurements up to 1 GeV/c not only to explore the kinematic dependence of the neutron A_N in the higher p_T region but also to study the $\sqrt{s}$ dependence by comparing the measurement result with that of PHENIX.

Analysis flow

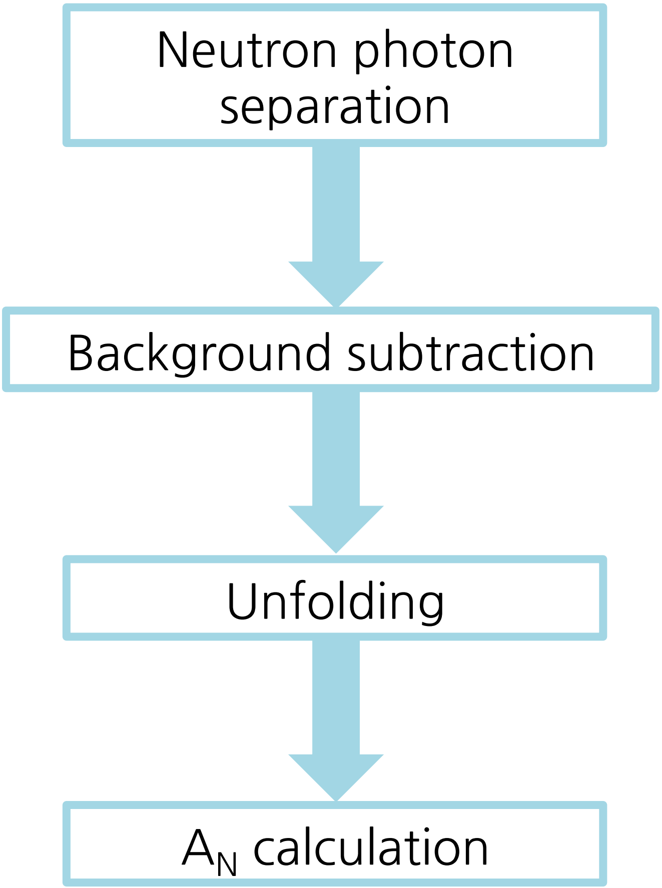

III. EVENT RECONSTRUCTION AND SELECTION

III. EVENT RECONSTRUCTION AND SELECTION

Before presenting the analysis cuts, the neutron and photon events are defined as follows. The neutron event is defined as there is a neutron produced by the collision heads towards the detector. When there is no neutron, the photon event is defined as at least one photon hits the detector. The neutron events were mainly measured by the so-called shower trigger that is activated when the energy deposits of any three consecutive GSO plates are larger than 45 MeV. Since the shower trigger is sensitive not only to the neutron events but also to the photon events, the neutron candidates were isolated by using the variable L_{2D} defined by

$$L_{2D} = L_{90\%} - 0.15 L_{20\%}, \quad (2)$$

where $L_{x\%}$ is defined by the longitudinal depth in the unit of the radiation length (X_0) with the accumulated energy deposition in the GSO plate being $x\%$ of the total. Fig. 2 (a) shows the $L_{90\%}$ versus $L_{20\%}$ distributions of the neutron and photon events in a Monte Carlo (MC) sample where the $p+p$ collisions were generated by QGSJET II-04 [12]. Fig. 2 (b) shows the L_{2D} distributions of both. An event was identified as a neutron if the L_{2D} was larger than $21X_0$. This threshold was optimized taking into account the neutron purity and efficiency which were estimated by GEANT4 [13] simulation with QGSP_BERT 4.0 model.

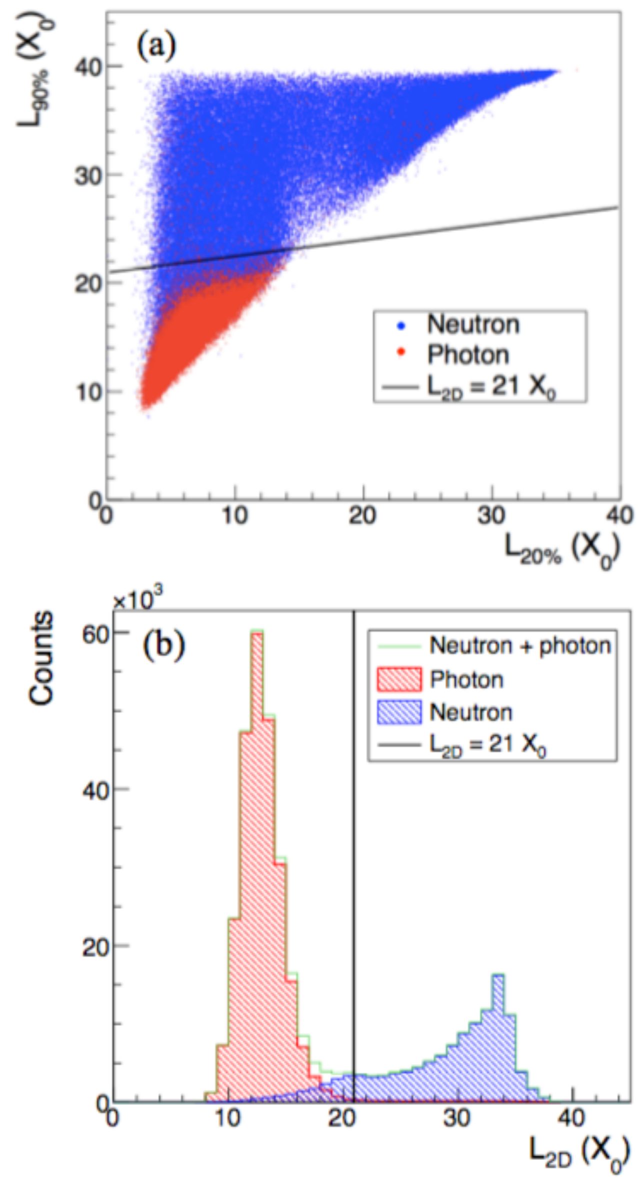

III. EVENT RECONSTRUCTION AND SELECTION

Hit positions of the neutrons were calculated by fitting the energy deposit distribution in the GSO bars using a Lorentzian-based function. The hodoscope layer with the maximum energy deposition was used for the position determination. The energy of neutron was reconstructed using a relation between the energy deposit sum of the GSO plates and the incident energy of neutron obtained by GEANT4 simulation. The position-dependent light collection efficiency and shower lateral leakage effect were also corrected in the simulation. Although the energy range was different, the above reconstructions were also applied for the previous analyses [14, 15] that used the RHICf detector. See Refs. [16, 17] for more details on the reconstruction and correction procedures.

In the GEANT4 simulation, 10^5 neutrons were generated to the center of the detector and their positions and energies were reconstructed as same as the data. For 200 GeV neutrons, energy and position resolutions of the RHICf detector were 1.1 cm and 37%, respectively. To improve the energy resolution, the hadronic showers developed in the deeper GSO plate were excluded by requiring $L_{90\%} < 37\ X_0$. The condition improved the energy resolution of neutrons at, e.g., 200 GeV, from 37% to 30%. The RHICf detector was located downstream of a RHIC dipole magnet, DX. Neutron hit was rejected if it was overlapped with the DX magnet shadow, or distance to the detector edge was smaller than 2 mm because of the poor performances in this region. In principle, only the neutral particles can reach the detector from the collision point because the DX magnet sweeps the charged particles. However, the detector can measure the charged particles when the neutral hadrons hit the DX magnet and create a hadronic shower. The events with the ADC values of FC larger than a fourth of the minimum ionizing particle (MIP) peak position were excluded to suppress the charged hadron background.

Analysis flow

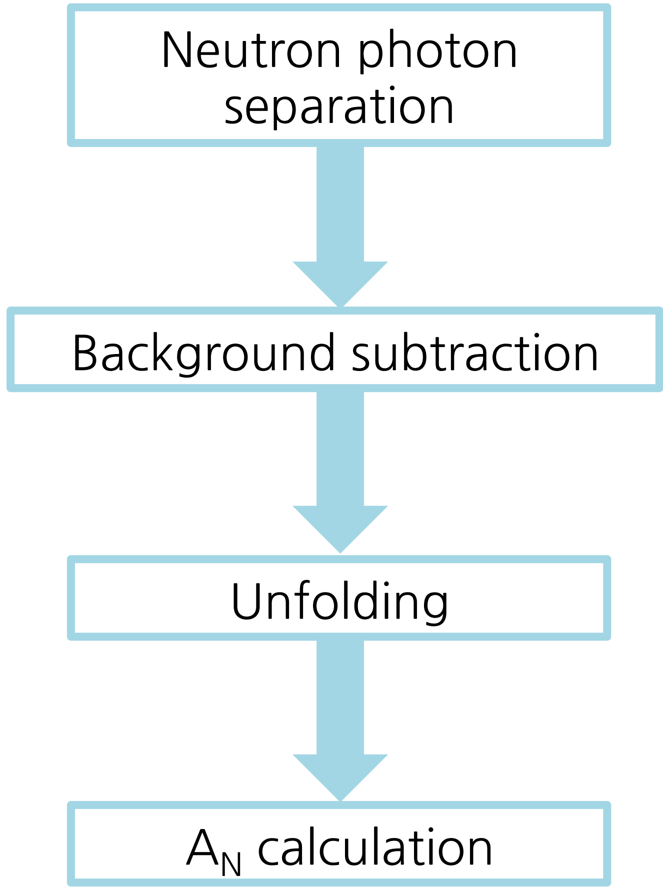

IV. BACKGROUND SUBTRACTION AND UNFOLDING

$$N^{\uparrow}_{\mathrm{neu}} = N^{\uparrow}_{\mathrm{trig}} - N^{\uparrow}_{\mathrm{pho}} - N^{\uparrow}_{\mathrm{cha}} \quad (6)$$

$$N^{\downarrow}_{\mathrm{neu}} = N^{\downarrow}_{\mathrm{trig}} - N^{\downarrow}_{\mathrm{pho}} - N^{\downarrow}_{\mathrm{cha}}, \quad (7)$$

where $N^{\uparrow(\downarrow)}_{\mathrm{trig}}$, $N^{\uparrow(\downarrow)}_{\mathrm{neu}}$, $N^{\uparrow(\downarrow)}_{\mathrm{pho}}$, and $N^{\uparrow(\downarrow)}_{\mathrm{cha}}$ are the number of triggered, neutron, photon, and charged hadron events, respectively, when the blue beam polarization is up (down). The charged hadron event is defined as at

---

least one charged hadron hits the detector when there is no neutron produced by the collision, that heads towards the detector. In order to estimate the $N^{\uparrow}_{\mathrm{pho}}$ and $N^{\downarrow}_{\mathrm{pho}}$, we performed a template fit of the L_{2D} distribution by scaling the neutron and photon events of the same kinematic bin in the QGSJET II-04 sample separately. Fig. 3 shows an example of the template fit. Negative neutron asymmetry and positive photon asymmetry from π^0 [11] can be seen by comparing the heights of each distribution. The photon contamination estimated by the template fit, which was less than 0.7%, was subtracted from the neu-

the MC event because the L_{2D} distribution of data is bigger than MC in $L_{2D} < 21$ in Fig. 3. Photon with higher energy shows larger L_{2D} value than the one with lower energy because more energy is deposited in the detector longitudinally. A_N difference between the two template fits after unfolding was negligible, which was less than 0.0007, thereby we did not consider the systematic uncertainty of the template fit.

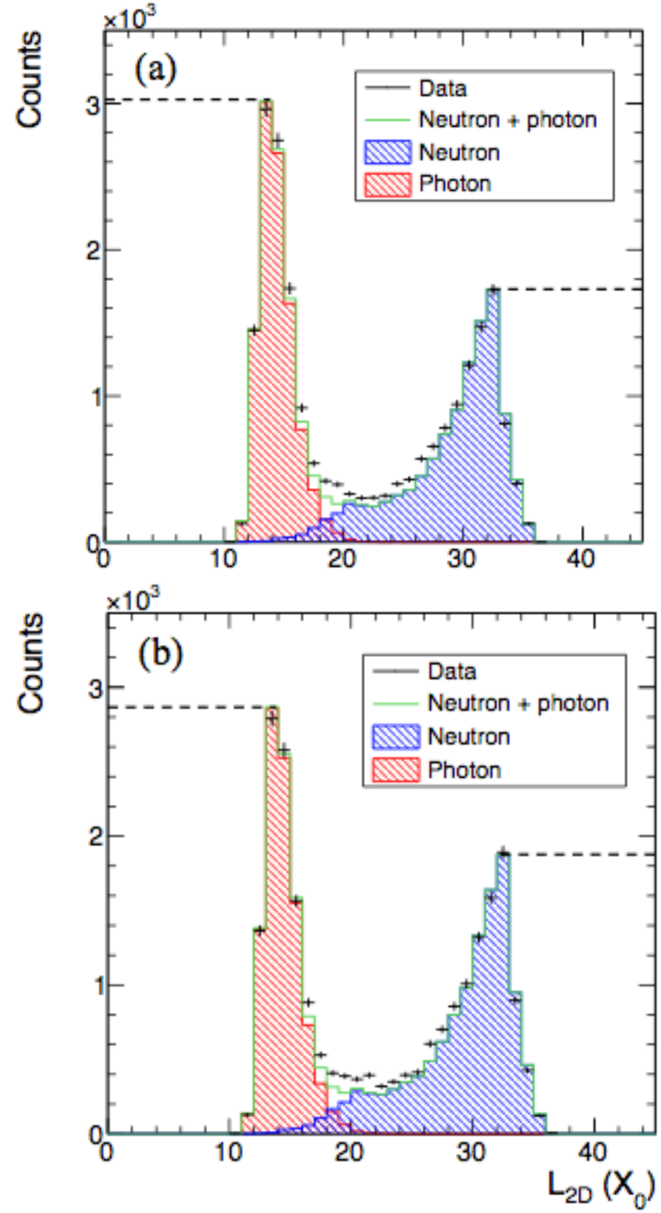

Template fit with the neighboring higher x_F bin

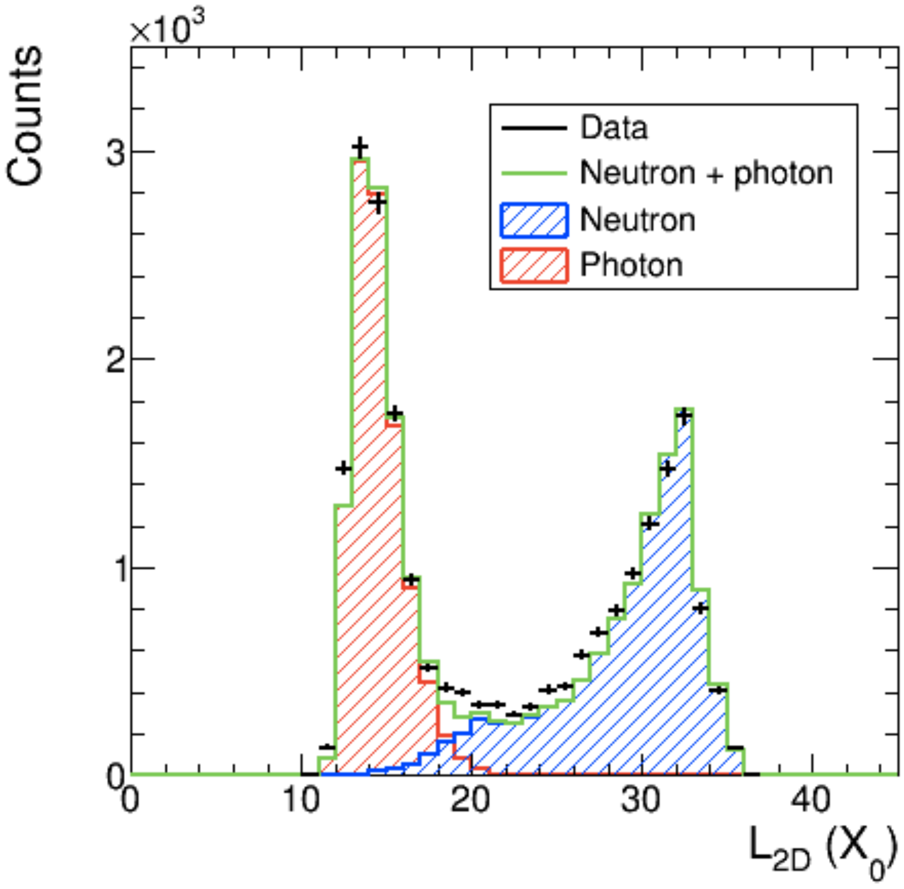

IV. BACKGROUND SUBTRACTION AND UNFOLDING

certainty of the template fit. Another template fit was performed to the ADC distribution of FC to estimate the $N_{\rm cha}^{\uparrow}$ and $N_{\rm cha}^{\downarrow}$ by scaling the neutron and charged hadron events of the same kinematic bin separately. Fig. 4 shows an example of the template fit. Average contamination of the charged hadron event in the neutron candidate was 0.2%, which was subtracted from the up and down polarization events separately. Since the template fit of the ADC distribution was an independent process of the one of the L_{2D} distribution and the contamination of the charged hadron event was less than that of the photon event, two cases were considered, (1) the charged hadron contamination was included in the photon, thereby only the photon contamination was subtracted and (2) there was no overlap between the two events, the two contaminations were subtracted separately. $A_{\rm N}$ difference between the two cases was negligible, which was less than 0.0004. Therefore, we also did not assign the systematic uncertainty to the process of the charged hadron subtraction. According to the QGSJET II-04, the neutron candidate was composed of the neutron (∼95.0%), lambda (∼3.5%), and neutral kaon (∼1.5%) after the background subtraction.

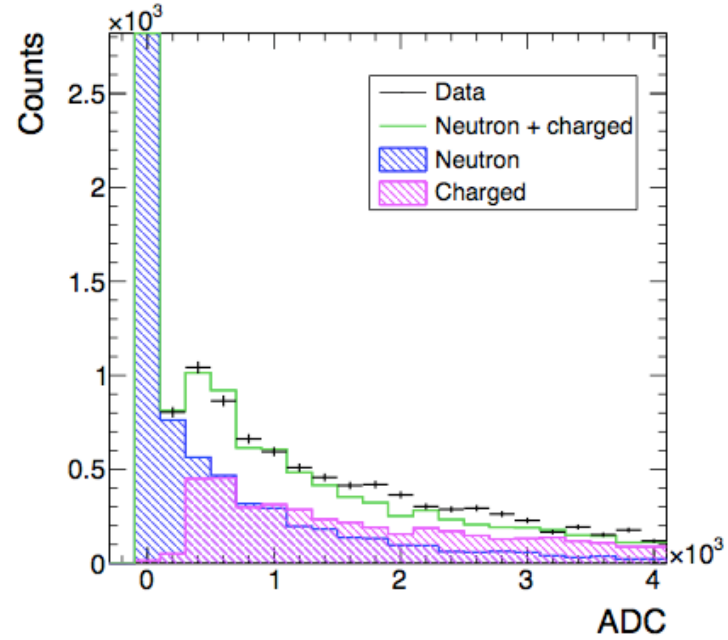

Analysis flow

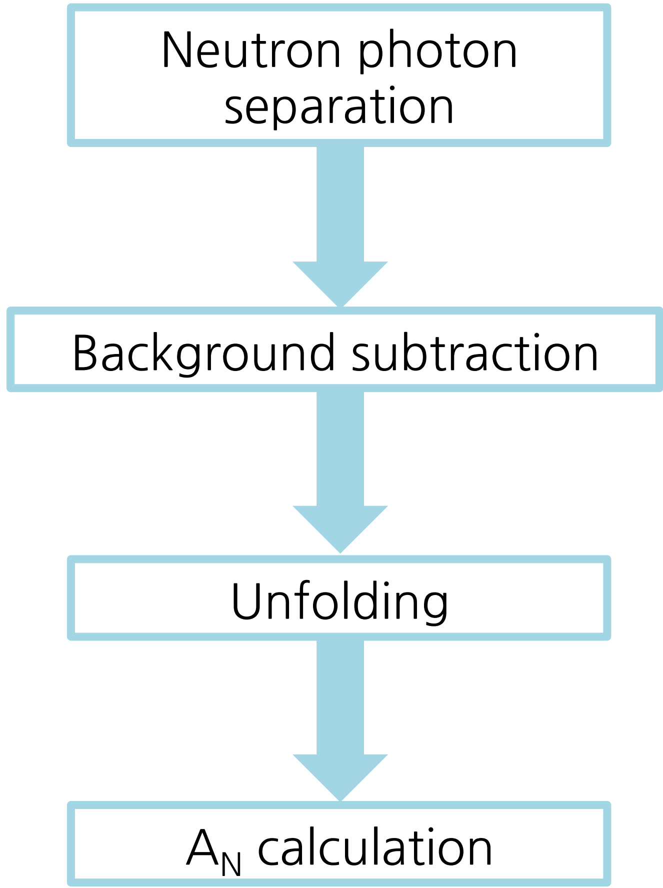

IV. BACKGROUND SUBTRACTION AND UNFOLDING

The kinematic values of neutron was unfolded by Bayesian unfolding method [20] using RooUnfold [21] package of ROOT [22]. For prior, a MC sample where the neutrons from 0 to 255 GeV were uniformly generated on the detector was used to avoid any bias from the particular particle productions. The iterative procedure was stopped when the χ^2 change between two outputs of consecutive iterations became smaller than 1. The variation of A_N by uncertainties of the unfolded data points was considered as one of the systematic uncertainties. We generated finite asymmetry by assigning up and down spin patterns in the QGSJET II-04 sample and confirmed that the unfolded spectra reproduced the input $\langle x_F \rangle$, $\langle p_T \rangle$, and A_N well within the total uncertainty that includes the statistical and systematic uncertainties. The differences between the reconstructed and input $\langle x_F \rangle$ and $\langle p_T \rangle$ were less than 0.04 and 0.02 GeV/c, respectively. Besides the systematic uncertainty of the unfolding process, the uncertainties of the beam center calculation and polarization estimation were considered. The beam center was measured by two methods [11]. Half of the A_N difference that was caused by two different beam centers was assigned as one of the systematic uncertainties. A_N variation by the systematic uncertainty of the beam polarization was also assigned to the systematic uncertainty.

V. RESULTS

V. RESULTS

Fig. 5, Table I, and Table II summarize the A_Ns for forward neutron productions as functions of $\langle x_F \rangle$ and $\langle p_T \rangle$. Fig. 5 (a) shows that the neutron A_N increases in magnitude with p_T, reaching about 0.2 at ∼0.8 GeV/c. Fig. 5 (b) shows that the backward A_Ns are consistent with zero. For the forward A_N, there is little x_F dependence in $p_T < 0.10$ GeV/c. However, as the p_T increases, clear x_F dependence is observed up to ∼0.7. Fig. 6 (a) and (b) show comparisons between the RHICf and PHENIX measurements. Absolute value of the A_N measured by the RHICf experiment is slightly larger than that of PHENIX in the highest kinematic bin, but the A_Ns of two measurements are consistent overall. The RHICf data is compared with the model calculation based on the π and a_1 exchange in Fig. 6 (c). The A_Ns are mostly consistent with the model calculation in $x_F > 0.6$. However, the model did not reproduce the A_Ns in $x_F < 0.6$ because of the existence of the x_F dependence.

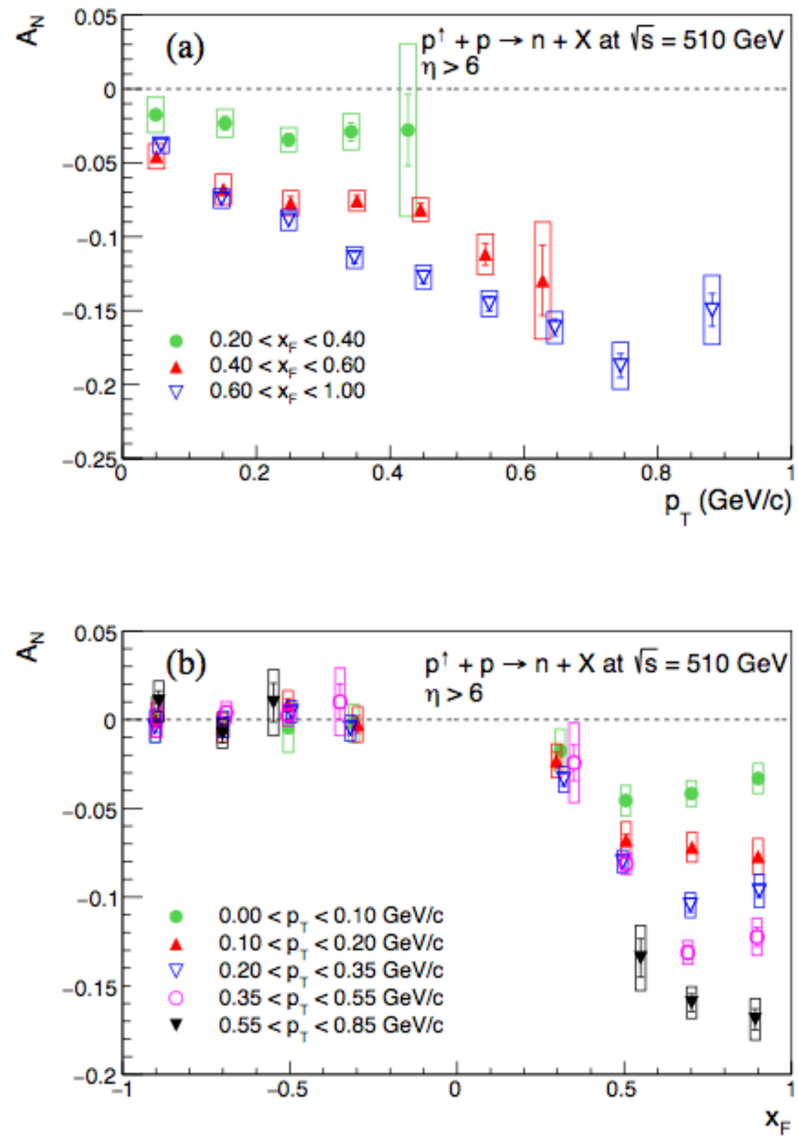

V. RESULTS

V. RESULTS

Fig. 5, Table I, and Table II summarize the A_Ns for forward neutron productions as functions of $\langle x_F \rangle$ and $\langle p_T \rangle$. Fig. 5 (a) shows that the neutron A_N increases in magnitude with p_T, reaching about 0.2 at ~0.8 GeV/c. Fig. 5 (b) shows that the backward A_Ns are consistent with zero. For the forward A_N, there is little x_F dependence in $p_T < 0.10$ GeV/c. However, as the p_T increases, clear x_F dependence is observed up to ~0.7. Fig. 6 (a) and (b) show comparisons between the RHICf and PHENIX measurements. Absolute value of the A_N measured by the RHICf experiment is slightly larger than that of PHENIX in the highest kinematic bin, but the A_Ns of two measurements are consistent overall. The RHICf data is compared with the model calculation based on the π and a_1 exchange in Fig. 6 (c). The A_Ns are mostly consistent with the model calculation in $x_F > 0.6$. However, the model did not reproduce the A_Ns in $x_F < 0.6$ because of the existence of the x_F dependence.

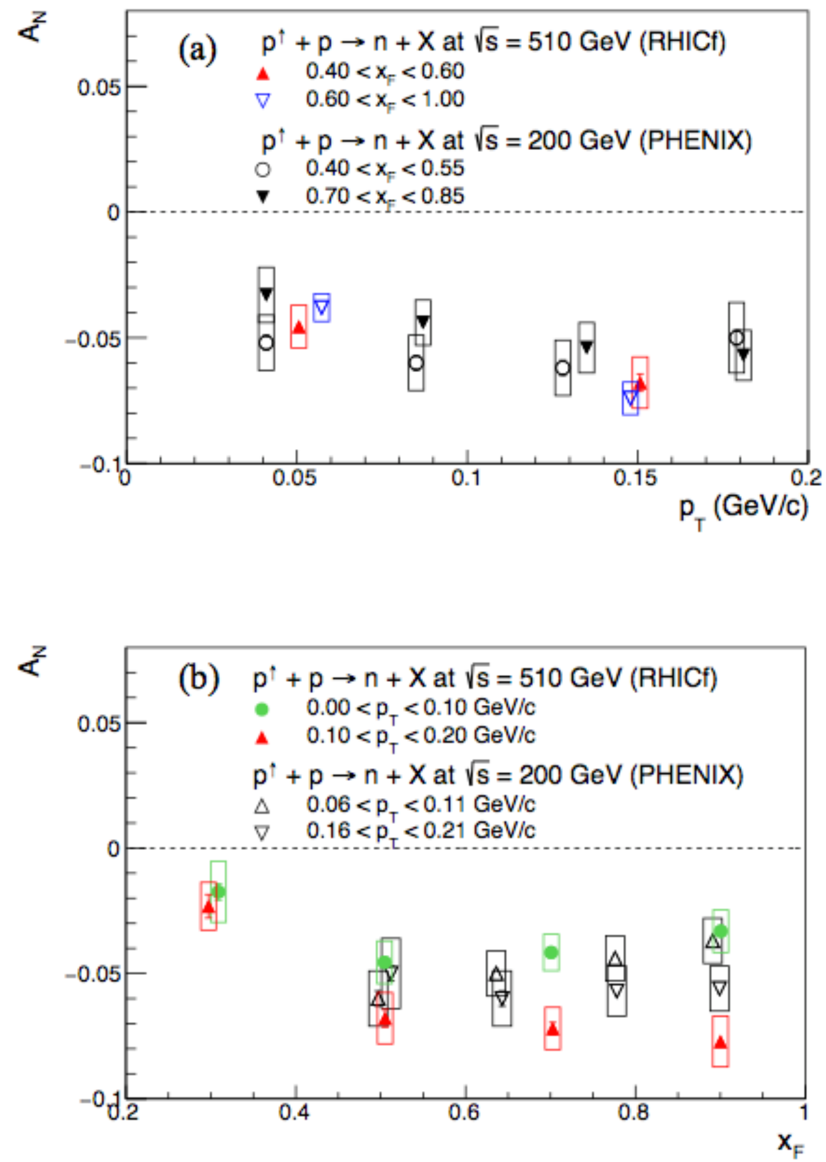

V. RESULTS

V. RESULTS

Fig. 5, Table I, and Table II summarize the A_Ns for forward neutron productions as functions of $\langle x_F \rangle$ and $\langle p_T \rangle$. Fig. 5 (a) shows that the neutron A_N increases in magnitude with p_T, reaching about 0.2 at $\sim$0.8 GeV/c. Fig. 5 (b) shows that the backward A_Ns are consistent with zero. For the forward A_N, there is little x_F dependence in $p_T < 0.10$ GeV/c. However, as the p_T increases, clear x_F dependence is observed up to $\sim$0.7. Fig. 6 (a) and (b) show comparisons between the RHICf and PHENIX measurements. Absolute value of the A_N measured by the RHICf experiment is slightly larger than that of PHENIX in the highest kinematic bin, but the A_Ns of two measurements are consistent overall. The RHICf data is compared with the model calculation based on the π and a_1 exchange in Fig. 6 (c). The A_Ns are mostly consistent with the model calculation in $x_F > 0.6$. However, the model did not reproduce the A_Ns in $x_F < 0.6$ because of the existence of the x_F dependence.

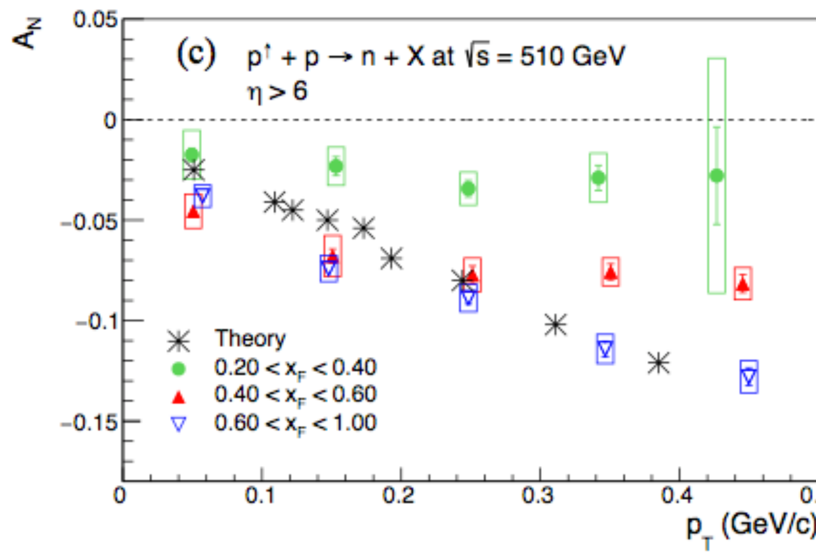

V. RESULTS

The π and a_1 exchange model partially reproduces the current results, but does not explain the x_F dependence. In Fig. 5 (a), A_Ns in $0.40 < x_F < 0.60$ and $0.60 < x_F < 1.00$ are consistent, but the x_F dependence is observed from ~0.3 GeV/c. In Ref. [7], spin effects by the absorptive corrections, which are initial/final state interactions, start to increase from ~0.2 GeV/c. However, it is expected that the absolute value of the neutron A_N is larger in $0.40 < x_F < 0.60$ than $0.60 < x_F < 1.00$. Other Regge poles like ρ and a_2 may enhance the asymmetry in $0.60 < x_F < 1.00$ because the spin effect by the ρ and a_2 exchange can make finite asymmetry in the higher x_F region [23]. More comprehensive theoretical considerations are necessary to understand the x_F dependence in $p_T > 0.3$ GeV/c. Since nothing of the Regge exchanges and absorptive corrections does not explain the x_F dependence in $p_T < 0.3$ GeV/c, a new production mechanism may be necessary to explain the present results.

From Kopeliovich's paper

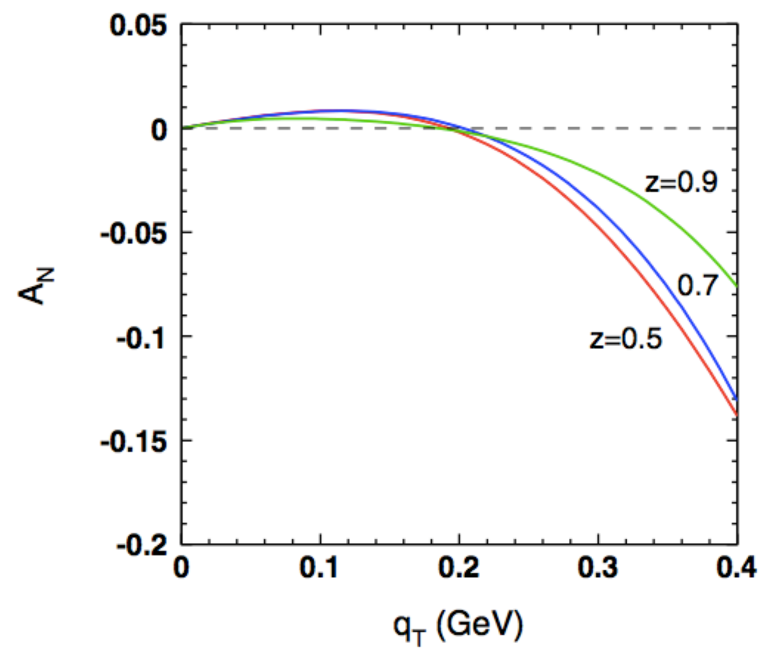

V. RESULTS

From Mitsuka-san's JPS slides

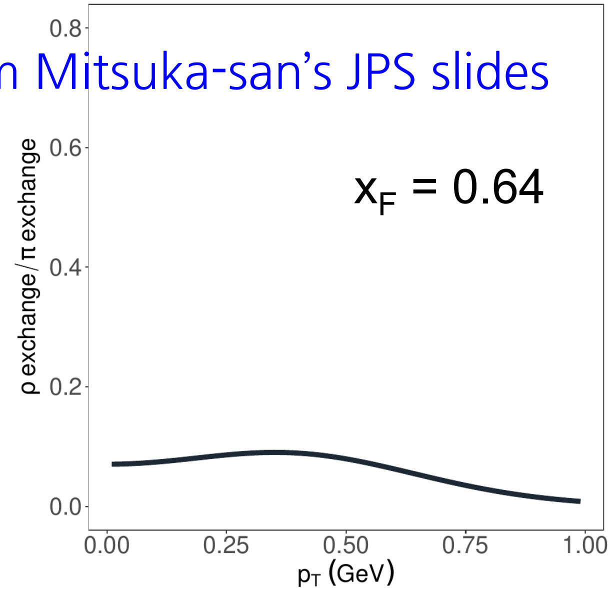

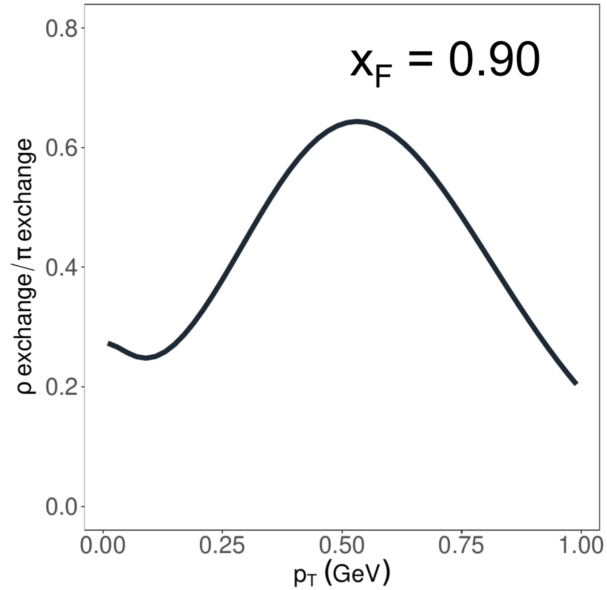

The π and a_1 exchange model partially reproduces the current results, but does not explain the x_F dependence. In Fig. 5 (a), A_Ns in $0.40 < x_F < 0.60$ and $0.60 < x_F < 1.00$ are consistent, but the x_F dependence is observed from ~0.3 GeV/c. In Ref. [7], spin effects by the absorptive corrections, which are initial/final state interactions, start to increase from ~0.2 GeV/c. However, it is expected that the absolute value of the neutron A_N is larger in $0.40 < x_F < 0.60$ than $0.60 < x_F < 1.00$. Other Regge poles like ρ and a_2 may enhance the asymmetry in $0.60 < x_F < 1.00$ because the spin effect by the ρ and a_2 exchange can make finite asymmetry in the higher x_F region [23]. More comprehensive theoretical considerations are necessary to understand the x_F dependence in $p_T > 0.3$ GeV/c. Since nothing of the Regge exchanges and absorptive corrections does not explain the x_F dependence in $p_T < 0.3$ GeV/c, a new production mechanism may be necessary to explain the present results.

Plan

- The paper will be submitted to PRD before SPIN2023 (Sep. 25-29) and the final result will be presented in the SPIN2023 and KPS Fall Meeting (Oct. 24-27).